

1820

The measurement of ultrasonic velocity [v_l] and echo-amplitudes [a_n] were carried out by Electronic Pulse Echo Selection (PES) method at a frequency of 2 MHz, supplied by innovative Instruments, Hyderabad, INDIA, and at different sintering temperatures. The PES technique is more accurate for measuring ultrasonic velocity and echo-amplitudes of low absorptive solids and liquids. The accuracy of the technique is 2 parts in 10^4 .



Figure 2: Transmitted pulse of Ultrasonic wave

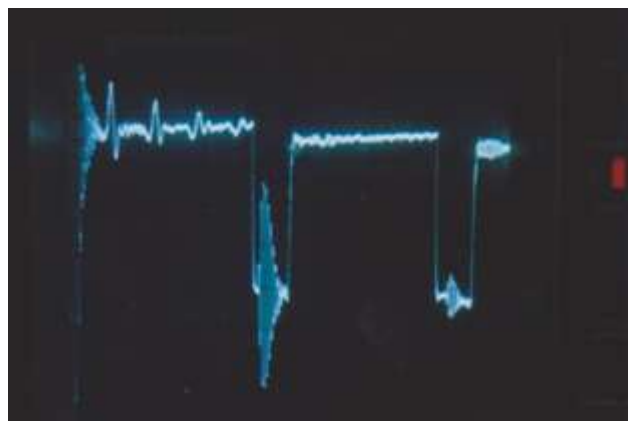


Figure 3: Two Selected echoes of Ultrasonic pulse.

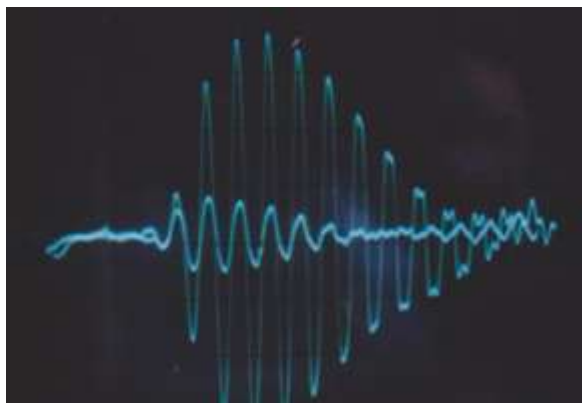


Figure 4: Overlapped echoes of Ultrasonic pulse.

The electronic circuitry required for PES technique consists of a high voltage pulse generator to excite the transducer, a continuous wave oscillator with high resolution a delayed strobe pulse generator to aid intensification of the trace and timer counter built into a single compact instrument as shown in Figure 1. In this method, a transducer of Lead Zirconate Titanate (PZT) X-cut for a longitudinal wave

having fundamental frequency 2 MHz is attached to one end of the sample holder.

The ultrasonic pulsed energy is transmitted by the transducer through the sample under test and gets reflected from the other end of the sample column and is being received by the sample transducer. Here the transducer acts both as transmitter and as a receiver. The echo pattern received by the transducer is fed to Cathode Ray Oscilloscope (CRO) after suitable amplification Figure 2. The delay between first two echoes are generally preferred as they are of higher amplitude and better resolved. Now removing Z-BNC from channel - B and connecting the same to Z-axis (for intensity modulation) to rear side of CRO. Now we see selected echoes on the screen Figure 3. Now to make measurements, one can approximate the travel time between two echoes selected for overlapping from the oscilloscope time scale. The travel time and amplitudes of different echoes are displayed on the timer and attenuation display. The X-BNC is connected to trigger mode of the CRO and the selection is achieved by the delays, as shown in Figure 4.

The longitudinal ultrasonic velocity, $v_l = \frac{2l}{T}$

where l – length of liquid column

T – travel time of ultrasonic wave

The Ultrasonic attenuation, $\alpha = \frac{\ln(\frac{a_0}{a_n})}{2ln}$

Where a_0 = the amplitude of transmitted pulse

a_n = amplitude of n^{th} echo

n = the number of echo

3. Results and Discussion

The ultrasonic properties of Mn-Zn ferrites with the addition of Bi_2O_3 and the sintering behaviour have been investigated by examination of density, ultrasonic velocity and attenuation measurements. The densities of Mn-Zn ferrites with various additive percentages of Bi_2O_3 as a function of sintering temperature are shown in Figure 1. It can be seen that the additive Bi_2O_3 enhances the sintered density. The density values for all the samples of Mn-Zn with Bi_2O_3 additive percentages of 0%, 0.003%, 0.006% and 0.015% were increasing trend.

It is clear that for pure Mn-Zn (with 0% Bi_2O_3), the sample density is increasing sharply from 900°C to 1075°C sintering temperature above which it becomes constant till 1200°C as shown in Figure 5. The ultrasonic velocity is also increasingly in a similar manner as the density which is shown in Figure 6. But it is found to be slow for 0.006% and 0.015% of Bi_2O_3 in Mn-Zn ferrite as shown in Figure 7 and 8. Figure 7 show a kink at about 925°C at which the additive 0.003% Bi_2O_3 takes a transition state from solid to liquid phase. But the Figure 8 of 0.015% Bi_2O_3 shows a sharpened kink at the same temperature.

The increased velocity and the sharpening of the kink at 975°C the lower temperature side is due to the fact that as the sintering temperature increases the interatomic distances decreases and the atoms become closer. Hence, the density

increases with this effect. This increased effect of density causes the ultrasonic velocity to increase in these samples of all compositions and pure Mn-Zn ferrite.

Table 1: Ultrasonic velocity, Density and Attenuation coefficient with different sintering temperatures and different additive % of Bi_2O_3 with Mn-Zn ferrite

Sintering Temperature	Attenuation coefficient	Velocity	Density
$T_s^\circ\text{C}$	α	$v_1\text{m/s}$	$\rho\text{ kg/m}^3$
975	3.89	5564.31	0.9825
1000	4.18	5925.27	0.9913
1025	4.41	6224.2	1.1025
1050	4.56	6531.55	1.3212
1075	4.64	6725.94	1.4728
1100	4.69	6754.6	1.5025
1125	4.7	6764.75	1.504
1150	4.71	6774.75	1.505
1175	4.71	6774.75	1.505
1200	4.71	6774.75	1.505
850	3.64	5040.31	0.9487
875	3.75	5569.14	0.9701
900	4.2	5887.05	0.985
925	4.45	6211.35	1.0725
950	4.59	6509.55	1.2215
975	4.64	6718.09	1.4602
1000	4.68	6770.46	1.4929
1025	4.7	6773.52	1.4972
1050	4.7	6773.08	1.4975
1075	4.7	6773.08	1.4975
1100	4.7	6773.08	1.4975
850	3.8	5225.21	0.9213
875	3.95	5631.08	0.9427
900	4.19	5924.27	0.9824
925	4.38	6587.45	1.0256
950	4.55	6623.02	1.3235
975	4.68	6689.18	1.3826
1000	4.71	6774.66	1.3945
1025	4.71	6775.68	1.3945
1050	4.71	6775.68	1.3945
1075	4.71	6775.68	1.3945
850	3.92	5345.65	0.902
875	4.18	5875.72	0.9225
900	4.33	6015.85	0.9438
925	4.52	6689.22	0.962
950	4.61	6692.28	0.988
975	4.68	6776.77	1.0325
1000	4.7	6820.05	1.3035
1025	4.71	6825.02	1.3256
1050	4.71	6825.02	1.3805
1075	4.71	6825.02	1.3805
1100	4.71	6825.02	1.3805

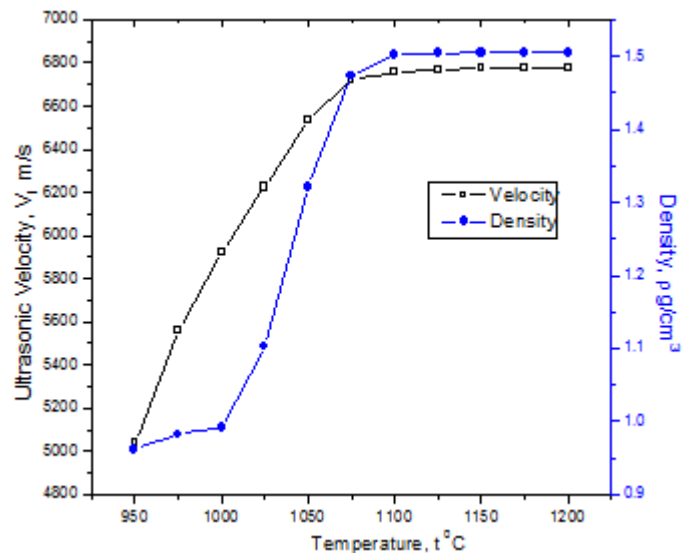


Figure 5: Variation of Ultrasonic velocity and density with sintering temperatures for additive percentage of 0% Bi_2O_3 in Mn-Zn ferrite.

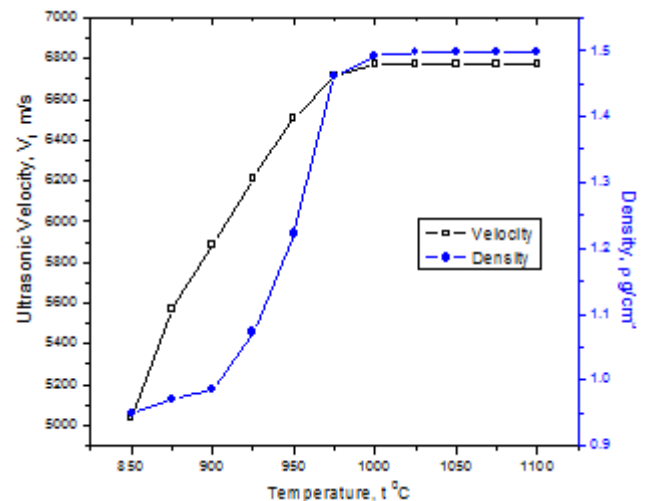


Figure 6: Variation of Ultrasonic velocity and density with sintering temperature for additive percentage of 0.003% Bi_2O_3 in Mn-Zn ferrite.

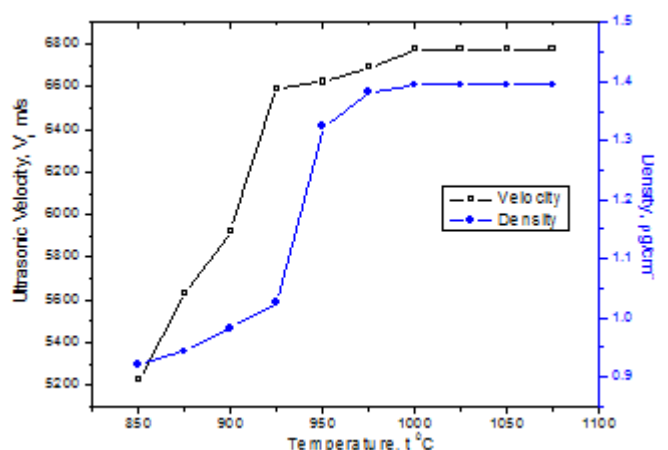


Figure 7: Variation of Ultrasonic velocity and density with sintering temperature for additive percentage of 0.006% Bi_2O_3 in Mn-Zn ferrite.

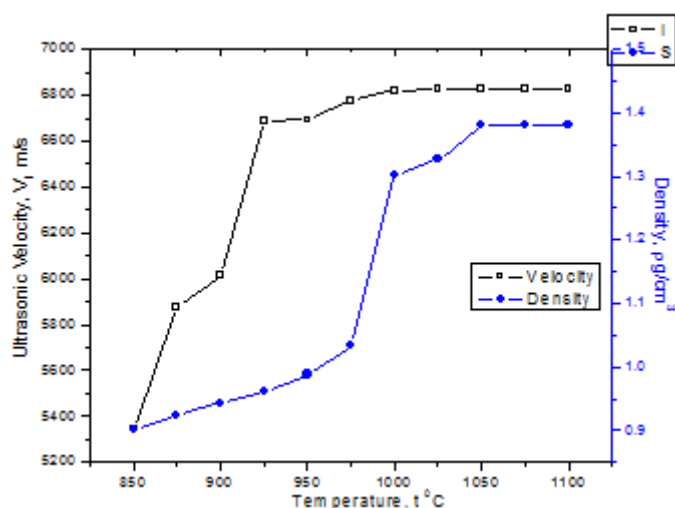


Figure 8: Variation of Ultrasonic velocity and density with sintering temperature for additive percentage of 0.015% Bi_2O_3 in Mn-Zn ferrite.

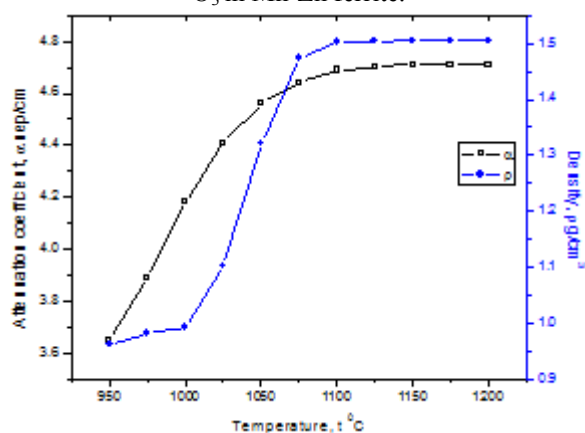


Figure 9: Variation of attenuation coefficient and density with sintering temperature for additive percentage of 0.003% Bi_2O_3 in Mn-Zn ferrite.

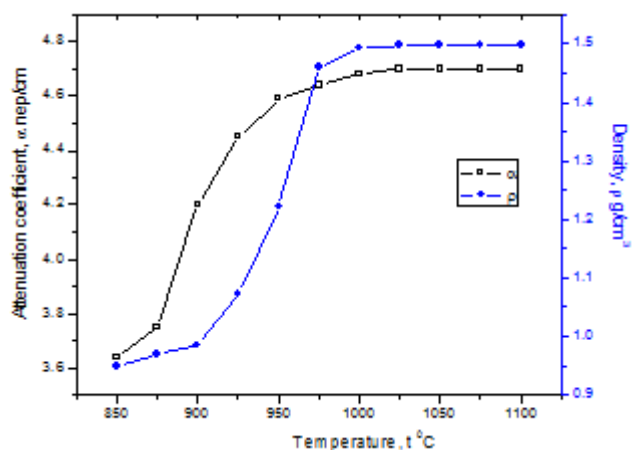


Figure 10: Variation of attenuation coefficient and density with sintering temperature for additive percentage of 0.003% Bi_2O_{3n} in Mn-Zn ferrite.

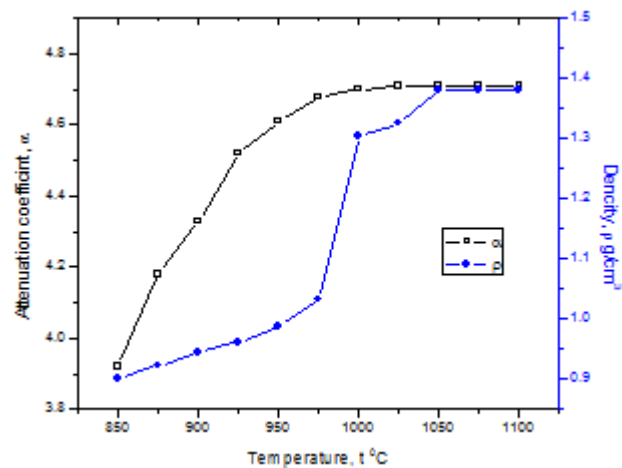


Figure 11: Variation of attenuation coefficient and density with sintering temperature for additive percentage of 0.006% of Bi_2O_3 in Mn-Zn ferrite.

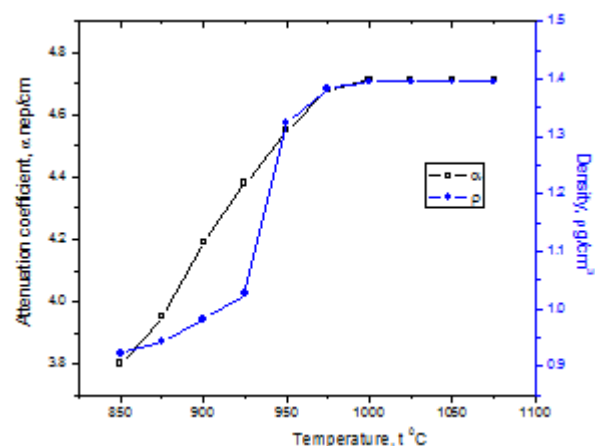


Figure 12: Variation of attenuation coefficient and density with sintering temperature for additive percentage of 0.015% Bi_2O_3 in Mn-Zn ferrite.

All Figures 9 to 12 of attenuation coefficient $[\alpha]$ and Density $[\rho]$ versus sintering temperature $[t]$ show that both values are increasing exponentially with sintering temperature. All the figures indicate that α is increased exponentially due the enhanced density which is due to the liquid phase transition at around 1075°C for pure Mn-Zn ferrite, 950°C in case of 0.015%, around 975°C for 0.006% of Bi_2O_3 and 1075°C for pure Mn-Zn ferrite.

It was reported [19] that the Bi_2O_3 particles exist as a liquid during the sintering, however, tend to segregate at grain boundaries leaving few micro voids in the grain when the T_s is low (below 1000°C) and the grain boundary mobility is small. Optimum addition [20] of Bi_2O_3 increases the permeability and saturation magnetic induction, at the same time it ensures good frequency stability of permeability.

The results indicate that Bi_2O_3 mainly segregates and concentrates in the grain boundary regions, promotes solid state reaction and grain growth, reduces porosity and enhances density.

4. Conclusions

The increasing trend of velocity and attenuation of ultrasound indicate that the additive Bi_2O_3 enhances the

sintering of Manganese Zinc by liquid phase transition which confirms the recent findings. The ultrasonic and magnetic properties can be improved by the optimum addition of Bi_2O_3 with Manganese Zinc Ferrite. Thus the Bi_2O_3 is a better additive to Mn-Zn ferrite used in the software and its ultrasonic application industry.

5.Acknowledgement

BRR is thank full to the University Grants Commission, New Delhi, India for their financial support for the Minor research project of UGC-SERO and also to Prof. V. Balasubramanian for providing the laboratory at P.G. College, Secunderabad, Osmania University, Hyderabad.

References

- [1] A. Globus, P. Duplex and M. Guyot, *IEEE Trans. MAG*, Vol. 7 (1971), pp. 617.
- [2] D.P. Rao, B.Ramesh, P.R.M. Rao, and S.B.Raju, *J.Alloys and Compounds*, vol. 282 (1999), pp.268.
- [3] G.C.Jain,B.K. Das, S. Kumari, *IEEE Trans. Mag*, vol.16(6), (1980), pp. 1428.
- [4] R.F. Sahoo, Englewood N.J. Cliffs, *Prentice Hall*, (1960), pp. 109.
- [5] J.E. Knowles, *Philips Tech. Rev.* vol. 24 (1968), pp. 242.
- [6] A.K. Mukhopadhyay, K.K. Phani, *J. Mat. Sci. Lett*, vol. 18 (1989).pp. 1759.
- [7] Usha Vasheny and Rajinder K. Puri, *IEEE Trans. MAG*, vol.25(4). (1989).
- [8] G.C. Jain, B.K. Das and N.C. Goel, *J. Amer. Ceram. Soc.*, vol. 62 (1979), pp.79.
- [9] L.M. Letyut, *Poroshkovaya Metallurgia*, vol.18 (1975), pp.59.
- [10] D.G. Wickham and H.B. Im, *U.S. Patent*, 3 (1967), pp.300.
- [11] T. Limura, *Jap. Yogo Kyokaishi*, vol. 84, (1976), pp. 34.
- [12] D. Ravinder, B. Ravinder Reddy, D. Linga Reddy, "Frequency Dependence of Ultrasonic behavior on mixed Nickel-Zinc Ferrites", *Mat. letters*, 49 (2001) pp.202.
- [13] H.T. Kim, H.B. Im, *J. of Mat. Scie.* 22 (1987), pp. 1235
- [14] B.V. Bhise, M.D. Dongare, S.A. Patil, S.R. Sawant, *J. Mat. Scien.Lett*, vol. 10, (1991), pp. 922.
- [15] H. Waqas, A.H. Qureshi, "Low temperature sintering study of man-sized Mn-Zn ferrites synthesized by sol-gel auto combustion process", *Journal of thermal analysis and calorimetry*, vol. 100 (2010) 2, pp. 529.
- [16] B Ravinder Reddy, D Linga Reddy and D Ravinder "Ultrasonic Investigation on Mixed Manganese-Zinc Ferrite", *Material Letters*, 56 (2002), 175-77.
- [17] H.B. Im, *Proc. Int. Conf.Ferrite*, Kyoto, Japan, 1980.
- [18] K. Janghorban, H. Shokrollahi, "Influence of V_2O_5 addition on the grain growth and magnetic properties of Mn-Zn high permeability ferrites", *J. of Mag. And Mag. Materials*, vol. 308 (2), 2007, pp. 238.
- [19] L.P. Martin, D. Dodden and M. Rosen, *J. Eur. Ceram. Soc.*, vol. 17 (1997), pp. 175.
- [20] H. Shokrollahi and K. Janghorban "Influence of additives on the magnetic properties, microstructure and densification of Mn-Zn soft ferrites", *Mat. Scie. and Engineering: B*, vol. 141 (2007) 3, pp. 91.

Figure Captions

- Figure 5: Variation of ultrasonic velocity and density of 0% Bi_2O_3 in Mn-Zn ferrite at different sintering temperatures.
- Figure 6: Variation of Ultrasonic velocity and density of 0.003% Bi_2O_3 in Mn-Zn ferrite at different sintering temperatures.
- Figure 7: Variation of Ultrasonic velocity and density of 0.006% Bi_2O_3 in Mn-Zn ferrite at different sintering temperatures.
- Figure 8: Variation of Ultrasonic velocity and density of 0.015% Bi_2O_3 in Mn-Zn ferrite at different sintering temperatures.
- Figure 9: Variation of attenuation coefficient and density of 0% Bi_2O_3 in Mn-Zn ferrite at different sintering temperatures.
- Figure 10: Variation of attenuation coefficient and density of 0.003% Bi_2O_3 in Mn-Zn ferrite at different sintering temperatures.
- Figure 11: Variation of attenuation coefficient and density of 0.006% Bi_2O_3 in Mn-Zn ferrite at different sintering temperatures.
- Figure 12: Variation of attenuation coefficient and density of 0.015% Bi_2O_3 in Mn-Zn ferrite at different sintering temperatures.